RSC Advances

ROYAL SOCIETY OF CHEMISTRY

www.rsc.org/advances

Journal Name

ARTICLE

Strong optical limiting behavior discovered in black phosphorus

Fang Zhang[a, b], Zhixin Wu[a, b], Zhengping Wang[a, b] †, Duanliang Wang[a, b], Shenglai Wang[a, b], Xinguang Xu[a, b]

Received 00th January 20xx,
Accepted 00th January 20xx

DOI: 10.1039/x0xx00000x

www.rsc.org/

Black phosphorous (BP), the most thermodynamically stable allotrope of phosphorus, fills up the lacuna left by other two-dimensional material with the band gap from 0.3 to 2 eV. The narrow direct band gap and the strong light-matter interaction make BP become a promising nonlinear optical (NLO) nano-material. In this paper, the NLO properties of multilayer BP nano-sheets were researched by open aperture Z-scan method. The optical limiting (OL) behavior was observed in BP material. Three different excitation wavelengths (1064, 532 and 355 nm) were used in the experiments, and the long wavelength excitation exhibited superior NLO performance, including OL and saturable absorption (SA). Our results demonstrate that BP is a promising candidate for OL applications.

Introduction

Due to the outstanding physical and chemical properties, atom-layer structure graphene overturned the traditional viewpoints on nanotechnology and opened the door to a new nano-world.[1] Graphene can offer extremely high charge mobility.[2] However, the intrinsic zero band gap structure makes graphene has many limitations for the electronic and photonic applications.[3-5]

Recently, the emergence of BP with band gap from 0.3 eV (bulk) to 2 eV (single layer BP or phosphorene) fills up the lacuna left by other 2D materials, including graphene, TMDCs, topological insulator and hexagonal boron nitride.[6-9] Meanwhile, strong excitonic effects are crucial in few-layer structures, reducing to the "optical gap" which has a smaller value[6]. The direct band gap and high mobility in few-layer BP semiconductor offer attractive prospect in future 2D electronic devices.[10-13] The band gap width of BP nano-sheets (BPns) depends on the number of layers, and the in-layer strain leads to a high mobility.[14] The direct transition enhances the interaction of light and material, and makes BPns are more suitable to be used as optoelectronic material compared to indirect band gap structure like MoS_2. The band gap of BPns can be continuously modulated by the strain and the external vertical electrical field,[15] which can be developed as solar cell.[16] The gate-tunable p-n diode based on p-type BP/n-type monolayer MoS_2 has been demonstrated.[17,18] Also a photo detector made of multilayer BPns has been used to record the diffraction-limited images of microscopic patterns in visible and near-infrared spectral regime.[19] Moreover, the over layers of insulating AlO_x, BN or other toughly oxidizable nano-materials can effectively restrain the ambient degradation caused by O_2 and saturated H_2O.[20,21] In short, BP makes up the disconnected band gap by graphene and TMDCs, and its adjustable direct band gap as well as high mobility demonstrate great potential for electronic and optoelectronic applications.

Unlike other 2D materials, few-layer BPns exhibit inherent anisotropic electronic and optoelectronic response due to the strong directional dependent absorption of BP crystal,[22,23] which is similar to the lower-symmetry bulk crystals.[24] The strong anisotropic, transient absorption responses allow people to easily identify the armchair and zigzag directions of BPns. The anisotropic, high-frequency intra-layer breathing modes can probe the crystalline orientation, too.[25] The low-frequency interlayer breathing modes (<100 cm^{-1}) are considerably more sensitive to interlayer coupling and their frequencies show a stronger dependence on the number of layers compared to high-frequency modes, which is an efficient means to probe the thickness of few-layer BPns.[25,26] The low-frequency interlayer breathing modes arise from the large interlayer force constant, which roots from the sizable covalent interactions between phosphorus atoms in adjacent layers which are not merely of the weak van der Waals force.[26] These strong interlayer interactions are important for electric-field induced formation of Dirac cone in BPns.

Now, nonlinear optical characteristics of BP have attracted extensive attentions. Lu et al. reported the broadband saturable absorption of multilayer BPns from visible (400 nm) to mid-IR (1930 nm) waveband.[27] Taking advantages of BP's saturable absorption, Q-switching and mode-locking have been realized for both of fiber lasers [28-33] and crystal lasers at

[a] State Key Laboratory of Crystal Materials, Shandong University, Jinan 250100, China.
[b] Key Laboratory of Functional Crystal Materials and Device, Shandong University, Ministry of Education, Jinan 250100, China.
† Corresponding author: zpwang@sdu.edu.cn.

different wavelengths.[34,35] Zheng et al. researched the optical limiting behavior of multilayer BPns in femtosecond laser[36]. In this paper, we researched the NLO properties of BPns from ultraviolet to near infrared waveband with open aperture z-scan technique. Different from reference[36] (the sample thickness was 33-53 nm), our sample was few layer with thickness of 7-10 nm. Besides, our excitation laser was picosecond pulse, however, the pulse of reference[36] is femtosecond laser. Moreover, our sample performed deeper modulation depth and larger two-photon absorption coefficient. Furthermore, compared to reference[36], we researched the influence of excitation wavelength to the nonlinear absorption and the results showed a great dependence of nonlinear behavior on wavelength. Our results open a new application for BP material, i.e. broad waveband OL of high power lasers.

Sample preparation

The original BP powder made from BP bulk crystal was purchased from Nanjing XFNANO Materials Tech Co. Ltd., China. The BPns was manufactured using liquid phase exfoliation (LPE), which is a simple and effective technique to prepare 2D nano-materials from the layered bulk crystals, such as graphene or TMDCs.[37] We chose IPA (isopropyl alcohol) as the organic solvent, which owns proper surface energy and can provide stable dispersion for layered materials compared to N-Methylpyrrolidone solvents (NMP) or ethyl alcohol (EA).[27] Figure S1 (supporting information) shows the detailed preparing processes of BPns. The dispersion liquid was diluted into three different concentrations with 0.50, 0.25 and 0.17 mg·mL^{-1}, which were denoted as sample 1#, 2# and 3#.

Characterization

To observe the morphology of the BPns, a scanning electron microscopy (SEM) measurement was conducted. The dispersion liquid was dripped on a pre-cleaned quartz substrate, and deposited in a vacuum device at room temperature to get rid of the residual solvent. After desiccation, the sample needed for SEM measurement was finished. Figure 1 (a_1) and 1 (b_1) were two typical SEM images of the as-prepared BPns, where the layered structure could be identified at the edge of the BPns. The BPns are in sizes of a few microns. Figure 2 (a_2) and 2 (b_2) were the amplified images, which exhibited relatively smooth surfaces. The granulum with sizes of several hundred nanometers on the surface was the accumulation of some small particles.

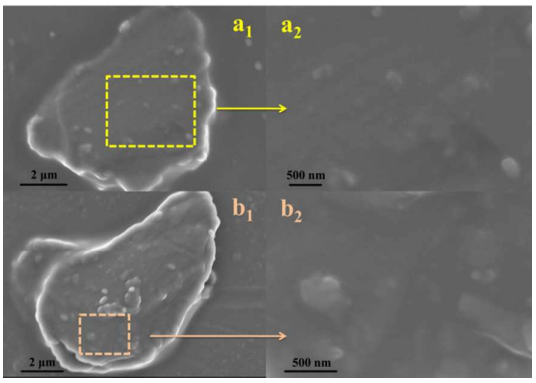

Figure 1. (a_1), (b_1): typical SEM images of BPns, (a_2), (b_2): the corresponding amplified images.

In order to determine the thickness of the BPns, an atomic force microscopy (AFM) measurement was carried out. As shown in Figure 2 (a) and 2 (b), the heights of three typical pieces of BPns were measured to be 10, 7 and 8 nm, respectively. Considering the aggregation effect during the deposition and the drying processes, the actual thicknesses of BPns in dispersion liquid might be smaller, which correspond to several atomic layers.

The linear absorption coefficient of BPns dispersion liquid can be determined from the transmission spectrum. In the spectral range of 350 to 1100 nm, by measuring the transmittance T of BPns plus quartz colorimetric utensil, and T_0 of the quartz colorimetric utensil, we can obtain the transmittance of the BPns by T/T_0. The results are shown in Figure S2 (supporting information). Due to the three samples with different concentrations exhibit the similar characteristics, the nonlinear results of 1# sample were chosen as representative and discussed in the following parts, so in Figure 2c we only display the linear transmittance of 1# sample. It can be seen that the BPns have a smooth transmission curve, which presents very small changes from UV to near infrared region. The linear absorption coefficients at 355, 532 and 1064 nm are calculated to be 5.98, 5.85 and 5.11 cm^{-1} for 1# sample.

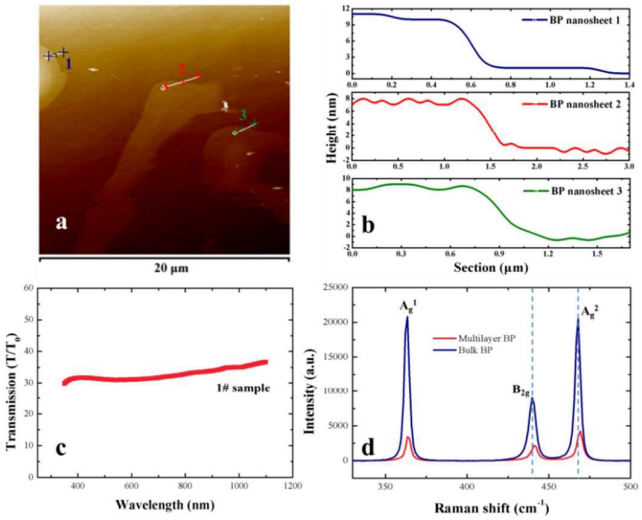

Figure 2. (a) Atomic force microscopy image, (b) Heights of three different BPns, (c) Transmission spectrum of the 1# BPns, and (d) Raman spectra of the original BP powder and the exfoliated BPns.

Raman spectra of original BP powder and BPns on quartz wafer were measured by Raman spectrometer (LabRAM HR800, HORIBA Ltd.) with a 633 nm excitation light. In Figure 2d, three well-known high-frequency (HF) characteristic peaks of BP at 363.5, 441.0 and 469.2 cm^{-1} were observed, which corresponded to the out-of-plane vibration mode (A_g^1), in-plane vibration modes along the zigzag direction (B_{2g}) and armchair direction (A_g^2), respectively.[25,27] It has been found that the dependence of HF vibration modes on the laser polarization can be used to determine the crystalline orientation of BP.[25] Compared to the original BP powder, the B_{2g} and A_g^2 vibration modes of BPns exhibit small blue shifts with the decrease of layer number, which also proves the few-layer characteristic of our sample. Compared to the HF vibration modes, the low-frequency (LF) interlayer phonon modes in BPns exhibit stronger dependence on thickness.[25,26] Limited by the instrument sensitivity, we didn't observe the LF phonon modes in this experiment.

NLO experiment

The open-aperture Z-scan method was used to examine the NLO response of the as-prepared BPns. The experimental setup was shown in Figure S3. The laser resource was a dye mode-locked Nd:YAG laser (PY61C-10, Continuum Inc, America) operating at 1064 nm, 40 ps pulses, with 10 Hz repetition rate. After frequency doubling and third harmonic generation, the pulse widths of 532 and 355 nm were 30 and 20 ps or so, respectively. The waist radius at the focus for 1064, 532 and 355 nm were 34, 29 and 25 μm, respectively.

Figure 3 exhibits the measurement results of 1# sample at different excitation wavelengths of 1064, 532 and 355 nm. Based on the single photon absorption (1PA), strong SA effect was observed at low power density. Subsequently, obvious OL behavior appeared when the power density reached to a certain level. When the intensity reached the threshold, the SA appeared at first and its magnitude elevated with the increasing of excitation intensity, which formed a raised package at the focus location. If further increase the introducing energy, the SA reached the maximum and then the 2PA induced OL process came on stage, which formed a pit on the raised package. At higher excitation energy levels, the magnitude of SA was suppressed, and the OL behavior gradually became the dominant NLO phenomenon. The maximum normalized transmittances of SA behavior with 1064, 532 and 355 nm excitations were 200%, 137% and 114% when the light intensities at the focus (z = 0) were 28, 69 and 201 $MW \cdot cm^{-2}$, respectively. The strongest OL depths at these wavelengths were 68%, 29% and 14% when the light intensities at the focus were 52, 114 and 306 $MW \cdot cm^{-2}$, respectively. More intensive OL behaviors were expected to occur if the laser intensity was elevated further. Due to the relatively small photon energy, the NLO behavior was much easier to be triggered by long wavelength laser excitation, i.e. the required light intensity was lower. As a comparison, no any nonlinear effects were observed from the dispersant solvent. In addition, the other two samples (2#, 3#) exhibited the similar disciplines as the 1# sample. The difference was that

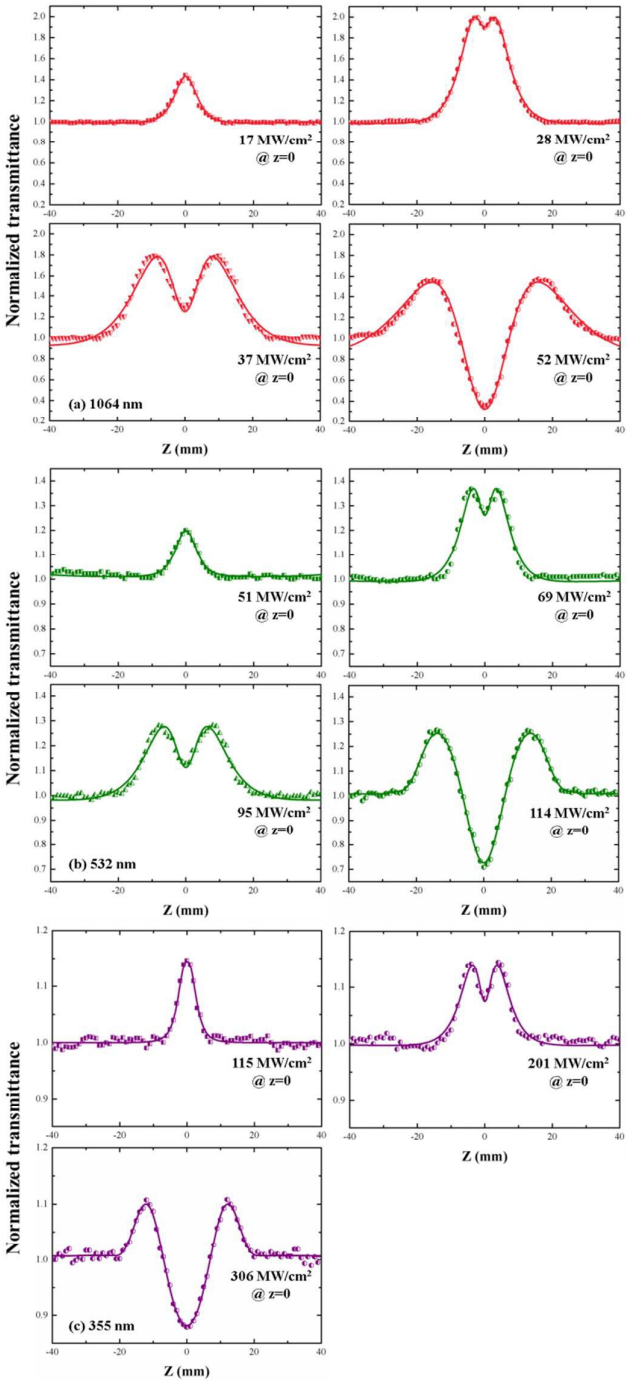

Figure 3. Open-aperture Z-scan measurement results of 1# sample at different excitation intensities (z=0) with excitation of (a) 1064, (b) 532 and (c) 355 nm lasers (the points are the experimental data and the solid lines are the fitted curves).

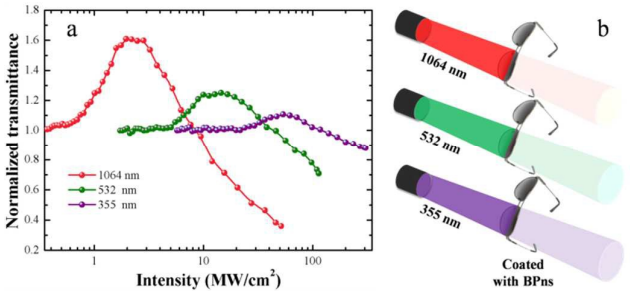

Figure 4. (a) Relationship between normalized transmittance of BPns dispersion and input laser intensity at 1064, 532 and 355 nm with peak power density (at z = 0) of 52, 114 and 306 MW·cm^{-2}, respectively; (b) Schematic diagram of the OL behavior in BPns for different laser wavelengths.

their modulation depths of SA and 2PA behaviors were relatively weaker at the same conditions.

Figure 4 (a) displays the relationship between normalized transmittance of BPns dispersion and input laser intensity at 1064, 532 and 355 nm with peak power density (at z=0) of 52, 114 and 306 MW·cm^{-2}, respectively. For each curve, the NLO process can be roughly divided into three stages, i.e. 1PA, 1PA plus 2PA, 2PA. The thresholds of 1PA induced SA at 1064, 532 and 355 nm excitations are 0.5, 5.1 and 21.7 MW·cm^{-2}, respectively. For 1064 nm excitation, when the excitation intensity varies from 0.5 to 1.8 MW·cm^{-2}, the SA is the dominated NLO effect. When the excitation energy is in the range of 1.8 - 2.8 MW·cm^{-2}, the SA and OL effects compete with each other and reach a relatively balance where the transmittance is unchanged basically. When the excitation energy exceeds 2.8 MW·cm^{-2}, the OL behavior becomes the main NLO effect. For 532 nm excitation, these three stages correspond to the excitation energy of 5.1 - 10.0 MW·cm^{-2}, 10.0 - 19.2 MW·cm^{-2}, and beyond 19.2 MW·cm^{-2}, respectively. For 355 nm excitation, they correspond to the excitation energy of 21.7 - 41.3 MW·cm^{-2}, 41.3 - 71.6 MW·cm^{-2}, and beyond 71.6 MW·cm^{-2}, respectively. In Figure 4a, the maximum normalized transmittances for 1064, 532 and 355 nm laser excitations are 161%, 125% and 111%, and the minimal normalized transmittances for them are 36%, 71% and 88%, respectively. Above results manifest that compared to the short wavelength excitation like 532, 355 nm, the long wavelength excitation like 1064 nm will bring stronger NLO responses including SA and OL effects, at lower power density. At the same time, the experimental results illustrate that by appropriately controlling the laser power density BPns can be selected to be the SA material or the OL material. The former has been used in passively mode-locking and Q-switching,[28-35] and the latter is hopeful to find important applications in protecting human eye or sensitive optical component from laser-induced damage. Figure 4 (b) is a schematic diagram for the OL application of BP material. It will be effective for broadband laser emissions from UV till to mid and far infrared, and be especially efficient for infrared lasers which are particularly dangerous because they are invisible to human eyes.

Discussion

The sample absorption obeys the law of $dI/dl=-\alpha(I)I$, where α is the absorption coefficient, and I is the light travelling distance. In the Z-scan measurement the normalized transmittance can be expressed as,[38]

$$T(z)=\sum_{m=0}^{\infty}\frac{\left(\frac{-\alpha I_0 L_{eff}}{1+z^2/z_0^2}\right)^m}{m+1} \quad (1)$$

where z is sample position, z_0 is the Rayleigh length of laser beam, α is the absorption coefficient, I_0 is the peak intensity at the focus (z=0), $L_{eff}=[1-\exp(-\alpha_0 L)]/\alpha_0$ is the effective length, α_0 is the linear absorption coefficient, L is the sample length. The excitation intensity I_z on the optical path is a function of z_0 and I_0, which is $I_z = I_0/(1+z^2/z_0^2)$. For a system where SA and OL coexist, the total absorption $\alpha(I)$ can be described as $\alpha(I)=\alpha_0/(1+I_z/I_s)+\beta I$, where β is the 2PA coefficient and I_s is the saturable intensity, defined as the optical intensity when the optical absorbance is reduced to one half of its unbleached value. The first term and the second terms on the right side of $\alpha(I)$ represent the SA and the 2PA, respectively. As introduced in part 3, the linear absorption coefficients α_0 of the BPns dispersion at 1064, 532 and 355 nm are 5.11, 5.85 and 5.98 cm^{-1}, respectively.

Based on above Equations, the theoretical fitting curves are obtained from the experimental points, as shown in Figure 3. It can be seen that they are in perfect agreements. The fitted saturable intensity I_s and 2PA coefficient β are shown in Figure 5, as well as table 1. The saturation intensity exhibits a dramatically decrease with the increasing of excitation wavelength. It means that the SA of BPns can be achieved more easily at long wavelength condition, which is favorable for Q-switching and mode-locking applications of infrared lasers. At the same time, the 2PA coefficient presents a rapid

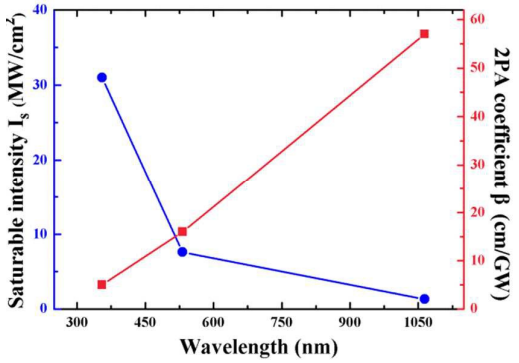

Figure 5. Relationships between excitation wavelength and saturable intensity, 2PA coefficient.

Journal Name

ARTICLE

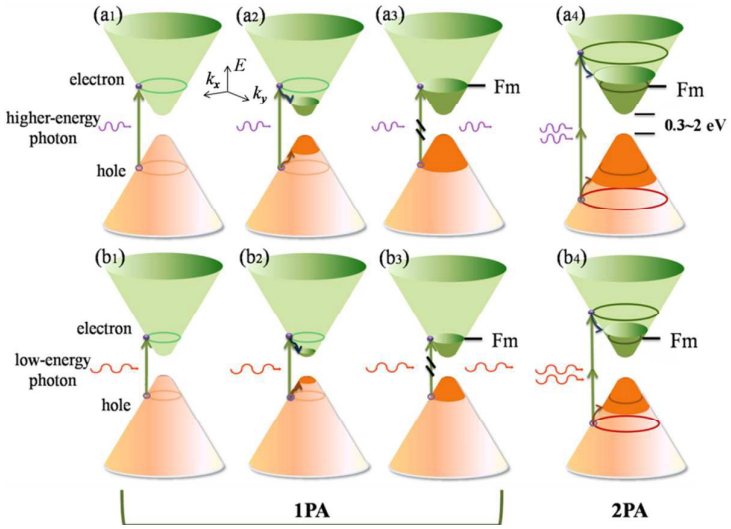

Figure 6. SA and OL mechanisms of BPns. (a) high energy (short wavelength) photon excitation. (b) low energy (long wavelength) photon excitation.

Table 1. Linear and NLO parameters of BPns.

λ (nm)	T (%)	α_0 (cm^{-1})	I_s ($MW \cdot cm^{-2}$)	β ($cm \cdot GW^{-1}$)	σ_{2PA} ($cm^4 \cdot s$)	$Im\chi^3$ $m^3(sW)^{-1}$	FOM $m^4(sW)^{-1}$
1064	36.0	5.11	1.3	57	1.07×10^{-47}	9.7×10^{17}	19.1×10^{14}
532	31.0	5.85	7.6	16	0.60×10^{-47}	5.5×10^{17}	9.3×10^{14}
355	30.3	5.98	31.0	5	0.28×10^{-47}	2.6×10^{17}	4.3×10^{14}

elevating with the increasing of excitation wavelength. Once again, it shows the superiority of BP as infrared OL material.

As shown in table 1, the saturable absorption intensities I_s of BP obtained in this work are on the level of $MW \cdot cm^{-2}$, which are much different from the previously reported values of 455.3 $GW \cdot cm^{-2}$ at 400 nm and 334.6 $GW \cdot cm^{-2}$ at 800 nm, respectively.[27] The great discrepancy maybe attributes to the sample parameters including the thickness of nano-sheets, dispersion concentration and interaction length in the colorimetric utensil, as well as the excitation conditions such as pulse duration. As we have discussed before, the I_s of two-dimensional material is quite different for steady state excitation and transient state excitation.[39]

The cross-section of 2PA ($\sigma_{2PA} = \hbar\omega\beta/N_0$, where $\hbar\omega$ is the excitation photon energy and $N_0 \approx 1.0\times10^{19}$ cm^{-3} is the density of BPns sample) are calculated to be 1.07×10^{-47}, 0.60×10^{-47} and 0.28×10^{-47} $cm^4 \cdot s \cdot photon^{-1}$ for 1064, 532 and 355 nm excitation, respectively. The imaginary part of the third-order NLO susceptibility, $Im\chi^3$, is directly related to the 2PA coefficient β. Their relationship is expressed as the Equation S1 of the supporting information. The Figure of merit (FOM) for the third-order optical nonlinearity is defined as FOM = $|Im\chi^{(3)}/\alpha_0|$. Referencing above results, $Im\chi^{(3)}$ and FOM of BPns for 1064, 532 and 355 nm excitations are calculated and listed in table 1.

For comparison, we also carried out a Z-san experiment for pure graphene under the same conditions. The excitation wavelength was 1064 nm, and the power density at the focus

(Z = 0) was 69 MW·cm^{-2}. The measurement result was shown in Figure S4 of the supporting information. The fitted saturable intensity I_s and 2PA coefficient β were 2.5 MW·cm^{-2} and 5.4 cm·GW^{-1}, respectively. Referencing table 1, we can see that BPns exhibite lower I_s and higher β than graphene does, i.e. presents stronger NLO effects.

The Figure 6 displays the energy level transitions of 1PA and 2PA in BPns. The SA effect is the consequence of 1PA process. Under the excitation of external laser, the electrons jump to the conduction band from the valence band, and subsequently cooled down in the constraint of the Pauli Exclusion Principle. When the incident intensity reaches the saturation intensity, the photo-carrier intensity is saturated and the remaining photons will transparently pass through, i.e. these photons will not be absorbed. To achieve the SA effect, the long-wavelength photon excitation requires a lower intensity to fully fill the lower energy levels compared to a short-wavelength photon excitation. When the excitation energy is increased further, two excitation photons tangle together and the electrons are stimulated into much higher energy levels. Accordingly, the transmittance declined rapidly. By comparing Figure 6 (a) with Figure 6 (b), one can see that for 2PA the long wavelength excitation corresponds to smaller energy band volume. It means that the 2PA of long wavelength excitation corresponds to fewer energy levels, i.e. fewer absorbed photon numbers. The small single photon energy and few absorbed photon numbers lead that the 2PA threshold of long wavelength excitation is obviously lower than that of short wavelength situation, at the same time the 2PA adjusting depth of long wavelength excitation is also larger. They are quite accordant with the experimental results in Figure 4 (a). The discrepancy between BPns and graphene can be roughly explained by the similar theory. Comparing with graphene, BP opens the zero band gap and decreases the energy band volume, correspondingly the threshold of nonlinear absorption is reduced. The experiment also proves the superiority of BP for NLO applications.

Conclusions

For liquid phase exfoliated BPns, the sizes and layer numbers were measured by AFM technique. A Z-scan equipment was used to research the NLO properties at different excitation wavelengths and intensity levels. For the first time, OL behavior was discovered in BP material. Compared to graphene, BP presents lower 1PA saturable intensity and larger 2PA coefficient. Our results indicate that BP is a promising OL material for various laser emissions, especially for invisible infrared lasers.

Acknowledgements

This work was supported by the National Natural Science Foundation of China (Grant No. 61178060), and Natural Science Foundation for Distinguished Young Scholar of Shandong Province (2012JQ18).

Notes and references

1 K. S. Novoselov, A. K. Geim, S. V. Morozov, D. Jiang, Y. Zhang, S. V. Dubonos, I. V. Grigorieva and A. A. Firsov, *Science* 2004, **306**, 666-669.
2 X. Du, I. Skachko, A. Barker and E. Y. Andrei, *Nat. Nano.* 2008, **3**, 491-495.
3 T. Ando, Y. Zheng and H. Suzuura, *J. Phys. Soc. Jpn.* 2002, **71**, 1318-1324.
4 A. B. Kuzmenko, E. van Heumen, F. Carbone and D. van der Marel, *Phys. Rev. Lett.* 2008, **100**, 117401.
5 Z. Q. Li, E. A. Henriksen, Z. Jiang, Z. Hao, M. C. Martin, P. Kim, H. L. Stormer and D. N. Basov, *Nat. Phys.* 2008, **4**, 532-535.
6 V. Tran, R. Soklaski, Y. Liang and Li Yang, *Phys. Rev. B* 2014, **89**, 235319.
7 X. Wang, A. M. Jones, K. L. Seyler, V. Tran, Y. Jia, H. Zhao, H. Wang, Li Yang, X. Xu and F. Xia, *Nat. Nanotech*. 2015, **10**, 517.
8 L. Liang, J. Wang, W. Lin, B. G. Sumpter, V. Meunier and M. Pan, *Nano Lett.* 2014, **14**, 6400−6406.
9 V. Tran, R. Fei and L. Yang, *2D materials* 2015, **2**, 044014.
10 M. Buscema, D. J. Groenendijk, S. I. Blanter, G. A. Steele, H. S. J. van der Zant and C. G. Andres, *NanoLett.* 2014, **14**, 3347-3352.
11 J. Na, Y. T. Lee, J. A. Lim, D. K. Hwang, G. T. Kim, W. K. Choi and Y. W. Song, *ACS Nano* 2014, **8**, 11753-11762.
12. Z. Yang, J. Hao, S. Yuan, S. Lin, H. M. Yau, J. Dai and S. P. Lau, *Adv. Mater.* 2015, **27**, 3748-3754.
13 T. Hong, B. Chamlagain, W. Lin, H. J. Chuang, M. Pan, Z. Zhou and Y. Q. Xu, *Nanoscale* 2014, **6**, 8978-8983.
14 H Liu, A. T. Neal, Z. Zhu, Z. Luo, X. Xu, T. David and P. D. Ye, *ACS Nano* 2014, **8**, 4033-4041.
15 Y. Li, S. Yang and J. Li, *J. Phys. Chem. C* 2014, **118**, 23970-23976.
16 J. Dai and X. C. Zeng, *J. Phys. Chem. Lett.* 2014, **5**, 1289-1293.
17 Y. Deng, Z. Luo, N. J. Conrad, H. Liu, Y. Gong, S. Najmaei, P. M. Ajayan, J. Lou, X. Xu and P. D. Ye, *ACS Nano* 2014, **8**, 8292-8299.
18 T. Hong, B. Chamlagain, T. Wang, H. Chuang, Z. Zhou and Y. Xu, "Anisotropic photocurrent response at black phosphorus–MoS_2 p–n heterojunctions," Nanoscale 2015, DOI: 10.1039/C5NR03400K.
19 M. Engel, M. Steiner and P. Avouris, *NanoLett.* 2014, **14**, 6414-6417.
20. J. D. Wood, S. A. Wells, D. Jariwala, K. S. Chen, E. Cho, V. K. Sangwan, X. Liu, L. J. Lauhon, T. J. Marks and M. C. Hersam, *NanoLett.* 2014, **14**, 6964-6970.
21 A. Avsar, I. J. Vera-Marun, J. Y. Tan, K. Watanabe, T. Taniguchi, A. H. Castro Neto and B. Özyilmaz, *ACS Nano* 2015, **9**, 4138-4145.
22 T. Hong, B. Chamlagain, W. Lin, H. Chuang, M. Pan, Z. Zhou and Y. Xu, *Nanoscale* 2014, **6**, 8978-8983.
23 F. Xia, H. Wang and Y. Jia, *Nat. Commun.* 2014, **5**, 4458-4464.
24 J. He, D. He, Y. Wang, Q. Cui, M. Z. Bellus, H. Chiu and H. Zhao, *ACS Nano* 2015, **9**, 6436-6442.
25 X. Ling, L. Liang, S. Huang, A. A. Puretzky, D. B. Geohegan, B. G. Sumpter, J. Kong, V. Meunier and M. S. Dresselhaus, *NanoLett.* 2015, **15**, 4080-4088.
26 X. Luo, X. Lu, G. K. W. Koon, A. H. Castro Neto, B. Özyilmaz, Q. Xiong and S. Y. Quek, *NanoLett.* 2015, **15**, 3931-3938.
27 S. B. Lu, L. L. Miao, Z. N. Guo, X. Qi, C. J. Zhao, H. Zhang, S. C. Wen, D. Y. Tang and D. Y. Fan, *Opt. Express* 2015, **23**, 11183-11194.

28 Y. Chen, G. Jiang, S. Chen, Z. Guo, X. Yu, C. Zhao, H. Zhang, Q. Bao, S. Wen, D. Tang and D. Fan, *Opt. Express* 2015, **23**, 12823-12833.
29 Z. C. Luo, M. Liu, Z. N. Guo, X. F. Jiang, A. P. Luo, C. J. Zhao, X. F. Yu, W. C. Xu and H. Zhang, "Micofiber-based few-layer black phosphorus saturable absorber for ultra-fast fiber laser," arXiv preprint, 2015, arXiv: 1505.03035.
30 D. Li, H. Jussila, L. Karvonen, G. J. Ye, H. Lipsanen, X. H. Chen an Z. P. Sun, "Ultrafast pulse generation with black phosphorus," arXiv preprint, 2015, arXiv: 1505.00480.
31 J. Sotor, G. Sobon, W. Macherzynski, P. Paletko and K. M. Abramski, "Black phosphorus - a new saturable absorber material for ultrashort pulse generation," arXiv preprint, 2015, arXiv: 1504.04731.
32 Z. Qin, G. Xie, H. Zhang, C. Zhao, P. Yuan, S. Wen and L. Qian, "Black phosphorus as saturable absorber for the Q-switched Er:ZBLAN fiber laser at 2.8 μm," arXiv preprint, 2015, arXiv: 1508.02850.
33 T. Jiang, K. Yin, X. Zheng, H. Yu and X. Cheng, "Black phosphorus as a new broadband saturable absorber for infrared passively Q-switched fiber laser," arXiv preprint, 2015, arXiv: 1504.07341.
34 B. Zhang, F. Lou, R. Zhao, J. He, J. Li, X. Su, J. Ning and K. Yang, *Opt. Lett.* 2015, **40**, 3691-3694.
35 R. Zhang, Y. Zhang, H. Yu, H. Zhang, R. Yang, B. Yang, Z. Liu and J. Wang, *Adv. Opt. Mater.* DOI: 10.1002/adom.201500298.
36 X. Zhang, R. Chen, G. Shi, J. Zhang, Z. Xu, X. Cheng and T. JiangI, *Opt. Lett.* 2015, **40**, 3480.
37 F. Bonaccorso and Z. Sun, *Opt. Mater. Express* 2014, **4**, 63-78.
38 S. B. Mansoor, A. A. Said, T. H. Wei, J. H. David and E. W. Stryland, *IEEE J. Quantum Electron.* 1990, **26,** 760.
39 F Zhang, S Han, Y Liu, Z Wang, X Xu, *Appl. Phys. Lett.* 2015, **106**, 091102.